We are IntechOpen, the world's leading publisher of Open Access books Built by scientists, for scientists

4,800
Open access books available

122,000
International authors and editors

135M
Downloads

Our authors are among the

154
Countries delivered to

TOP 1%
most cited scientists

12.2%
Contributors from top 500 universities

WEB OF SCIENCE™

Selection of our books indexed in the Book Citation Index in Web of Science™ Core Collection (BKCI)

Interested in publishing with us?
Contact book.department@intechopen.com

Numbers displayed above are based on latest data collected.
For more information visit www.intechopen.com

Chapter 1

Waveform Design and Related Processing for Multiple Target Detection and Resolution

Gaspare Galati and Gabriele Pavan

Additional information is available at the end of the chapter

http://dx.doi.org/10.5772/intechopen.71549

Abstract

The performance of modern radar systems mostly depends on the radiated waveforms, whose design is the basis of the entire system design. Today's coherent, solid-state radars (either of the phased array type or of the single-radiator type as air traffic control or marine radars) transmit a set of deterministic signals with relatively large duty cycles, an order of 10%, calling for pulse compression to get the required range resolution. Often, power budget calls for different pulse lengths (e.g., short, medium, and long waveforms with a rectangular envelope) to cover the whole radar range. The first part of the chapter includes the topic of mitigating the effect of unwanted side lobes, inherent to every pulse compression, which is achieved both by a careful and optimal design of the waveform and by a (possibly mismatched) suitable processing. The second part of the chapter deals with the novel noise radar technology, not yet used in commercial radar sets but promising: (1) to prevent radar interception and exploitation by an enemy part and (2) to limit the mutual interferences of nearby radars, as in the marine environment. In this case, the design includes a tailoring of a set of pseudo-random waveforms, generally by recursive processing, to comply with the system requirements.

Keywords: radar pulse compression, noise radar technology

1. Introduction

The main concern of radar signal processing is the extraction of useful information (generally referred to as "targets") from the background and disturbance of various kinds (noise, clutter, and jammer) [1, 2]. A typical processing input to a surveillance (or search) radar is the set of echoes from a point target at the generic reference position, which, for the two-dimension (2D) case, are naturally organized in *Range* (fast time) and in *Azimuth* (slow time), see **Figure 1**. **Figure 2** shows a real case of plan position indicator (PPI) acquisition.

IntechOpen

© 2018 The Author(s). Licensee IntechOpen. This chapter is distributed under the terms of the Creative Commons Attribution License (http://creativecommons.org/licenses/by/3.0), which permits unrestricted use, distribution, and reproduction in any medium, provided the original work is properly cited.

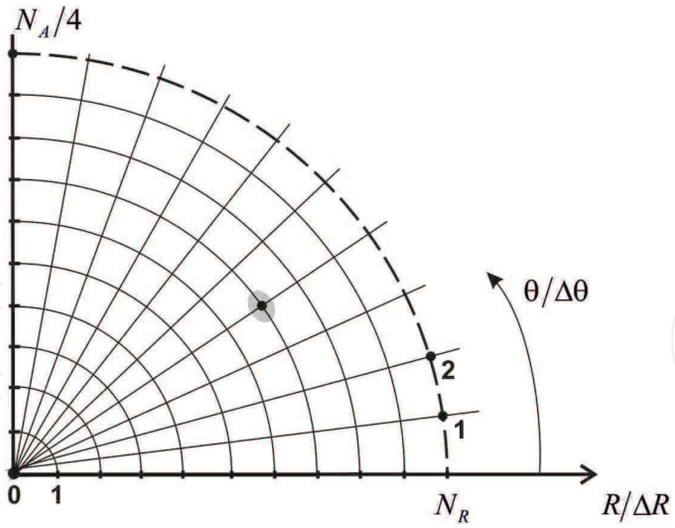

Figure 1. Range-Azimuth point target. $\Delta\theta$ = Azimuth resolution, ΔR = range resolution, N_A = number of azimuth cells, and N_R = number of range cells.

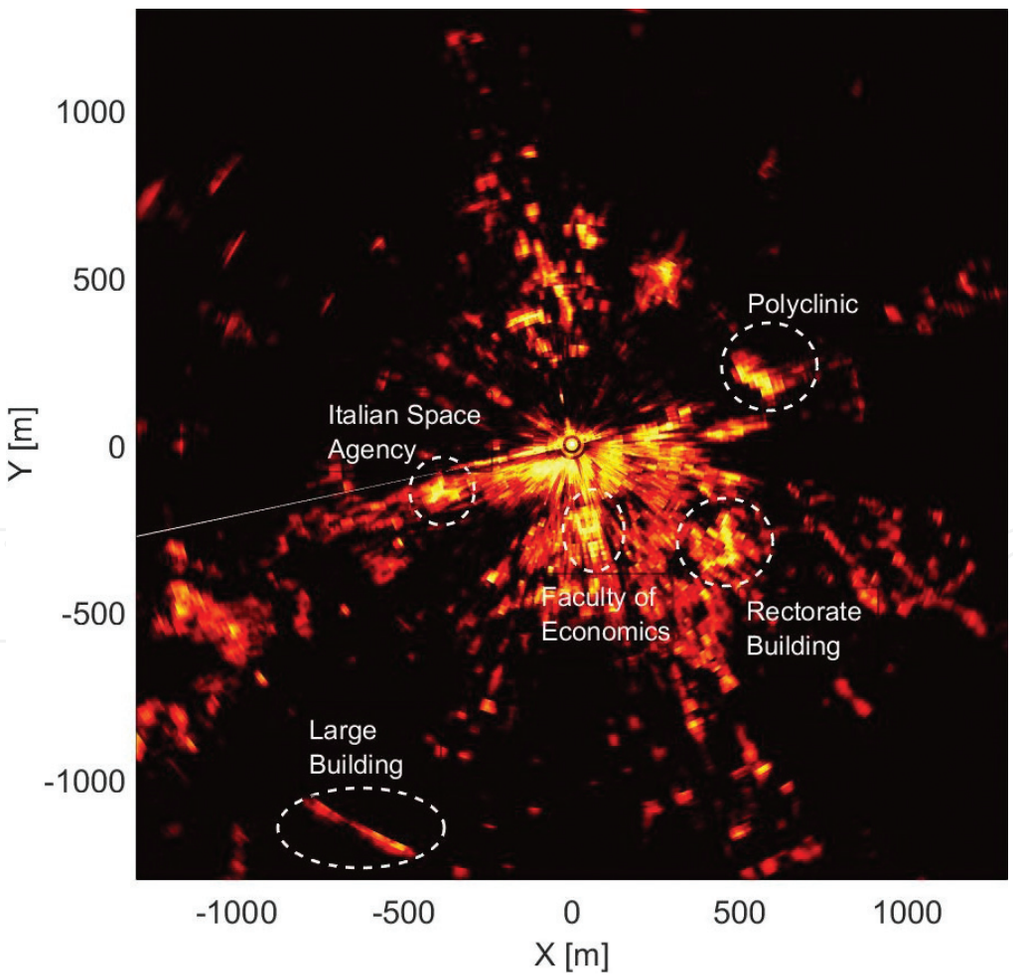

Figure 2. Real case of PPI acquisition (Tor Vergata University area).

The status of electronic technology of early radars of the World War II (WWII) period brought the designers to use simple waveforms, that is, rectangular pulses and sequences of them. Very soon, they understood that a receiver bandwidth *matched* to the transmitted pulse, that is, roughly equal to the reciprocal of the pulse duration, maximizes the output signal to noise ratio or *SNR* [3, 4]. The *Range* resolution, ΔR, is a function of the pulse duration τ, expressed in distance units, that is:

$$\Delta R = c\tau/2 \tag{1}$$

where $c = 2.99792 \times 10^8\ m \cdot s^{-1}$, which is the speed of light. In order to cope with the conflicting requirements of increasing the average power, proportional to the pulse duration, while maintaining a fair *Range* resolution, *Pulse Compression* techniques were devised and applied after WWII both in the USA and in the Soviet Union [5, 6]. These techniques use sophisticated waveforms in the place of the simple, rectangular pulse, with matched filtering (with sometimes a wanted mismatching). The early waveforms, still used today, were mostly based either on bi-phase coding, for example, Barker [7], or on the even most popular frequency modulation (FM or LFM in the linear case), also known as *chirp* signal [8, 9].

Historically, the design of the chirp radar in the Western world was made public in the 1960s [8] and, in the Eastern world, in the works (1950s) by Yakov Shirman[1] [11].

The radar signals synthesis problem was first examined by the ambiguity function (AF), introduced by Woodward in the 1950s [12]. Basically, the AF is a two-variable real function representing the modulus (sometimes the squared modulus) of the matched filter output when at the input there is a delayed and Doppler-shifted replica of the radar waveform. In the following, we assume the widely used correlation processor in radar reception, which is equivalent to the above-discussed matched filter (MF). The AF allows us to quantify the distribution in *Range* (i.e., delay) and in radial velocity (i.e., Doppler frequency) of the interference level due to point scatterers outside the reference delay-Doppler cell (i.e., the cell in which a target is to be detected and located). In the 1960s and 1970s, there were many attempts to use the AF to design radar waveforms with "good" characteristics, that is, "low enough" sidelobes in *Range* (and in radial velocity) and "well shaped" mainlobe (i.e., a narrow peak). Such specifications, referred to the envelope of the matched filter output, did not led to significant results in terms of practical waveforms design. Not only because the phase was ignored in them but, mainly, because a waveform designed according to a specific ambiguity function, for example, a "*thumbtack*" shaped one, might be hardly implementable in a real radar for various reasons, first of all the relevant need to transmit constant-modulus signals to maximize the energy radiated on the target and hence, the detection capability. In fact, dynamic range is another constraint to be carefully considered in addition to eclipsing losses, to coding accuracy, and so on. The interest in the AF has reoccurred in the 1990s and 2000s with the studies of multiple transmitters and multiple receivers' radar as a multiple input multiple output (MIMO) system [13–16], often named *netted*, *multistatic,* or *multisite*, as well as with studies of

[1]Y. Shirman received the IEEE Pioneer Award in 2009 "For the independent discovery of matched filtering, adaptive filtering, and high-resolution pulse compression for an entire generation of Russian and Ukrainian radars" [10].

integration of telecommunication capabilities in radars [17]. These systems call for waveforms designed and optimized in order to get a low Peak Side-Lobe Ratio (*PSLR*), good orthogonality properties, and a low degradation in the mainlobe, that is, low *SNR* loss (typically 1–2 *dB*, depending on the weighting function used). Considering that a single *dB* of additional *SNR* gained is nearly equivalent to a 25% increase in the transmitter power, for cost-effective solutions it is relevant to avoid these losses due to the weighting.

Concerning the waveforms selection and the related matched filter (MF), we can distinguish among: (1) rectangular pulse, (2) deterministic single code (Barker, Frank, Chirp,…), and (3) multiple codes, whose extent may theoretically reach an infinity number of signals (MIMO, noise radar).

In case (1), after a first analog (radio frequency (RF) or intermediate frequency (IF)) filtering before the analog-to-digital (A/D) conversion to limit the useful band and to suppress the thermal noise, an approximation of the rectangular MF is usually implemented using a Bessel filter, followed by sampling and A/D conversion (about two samples for a pulse).

In case (2), after sampling and A/D conversion of the sub-elements of the code (chips), a digital MF to the code is used: if $x[n]=x(nT)$ is the sequence of the samples of $x(t)$ obtained with a sampling period T, then the digital impulse response $h[k]$ of the digital filter is $x^*[N-n]$ where N is an integer equal or greater than the length of the numeric code.

In case (3), it is suitable to carry out directly the correlation between the received signal and the stored replica of the transmitted signal, which could vary each waveform repetition time (WRT) or each group of WRT. The fastest operation is in the frequency domain multiplying the spectrum of the signals (fast Fourier transform [FFT] and "zero padding") to obtain the aperiodic convolution/correlation. The algorithm is conceptually simple and compatible with the modern processing means also for high sample rates (in the order of hundreds of mega samples/second). It is based on the following steps: (1) computation, by FFT, of the Fourier transform of the received and reference signals, that is, $X(f)$ and $H(f)$, respectively; (2) after "zero padding" multiplication of $X(f)$ by the conjugate $H^*(f)$; and (3) inverse fast Fourier transform (IFFT) of the previous product.

In the following, we present the main characteristics of both deterministic and random signals and their comparison, including an analysis of the auto and cross-correlation functions and spectral properties, with recommendations for their practical use.

2. Waveform requirements

In the following, we will consider both *continuous-time* signals with duration T, that is, of the type $s(t)$ for $0<t<T$ with mean power $\frac{1}{T}\int_0^T |s(t)|^2 dt$, and *discrete-time* signals of the type s_k for $1\le k\le N$ with mean power $\frac{1}{N}\sum_{k=1}^{N} |s_k|^2$. We consider the main requirements of a set of M signals with complex envelope $s_i(t)$ for $i=1,\ldots,M$, pulsewidth T, same power, and band B. For each signal (we drop the index i in the following), they are defined by:

- $PSLR = \frac{\max_k(\tilde{s}_k)}{\max_k(m_k)}$ and Integrated Side-Lobe Ratio $(ISLR) = \frac{\sum_k |\tilde{s}_k|^2}{\sum_k |m_k|^2}$ where $\tilde{s}_k$ and m_k, are respectively the sidelobe and the mainlobe samples of the autocorrelation of $s(t)$.
- Crest factor C (or peak-to-average ratio, PAR): $C = PAR = \frac{max_k(|s_k|)}{\sqrt{\frac{1}{N}\sum_{k=1}^{N}|s_k|^2}}$ where N is the number of signal samples. C is the peak amplitude of the waveform divided by the *rms* value of the waveform.
- Mean envelope-to-peak power ratio $(MEPPR) = \frac{\frac{1}{N}\sum_{k=1}^{N}|s_k|^2}{max_k\left(|s_k|^2\right)}$, where $MEPPR = \frac{1}{C^2}$.

To evaluate the orthogonality between the signals $s_i(t)$ and $s_j(t)$, the normalized cross-correlation is defined as:

- $r_{ij}(t) = \frac{|R_{ij}(t)|}{|R_{i(j)}(0)|}$ where $R_{ij}(t) = \int s_i^*(\theta)s_j(t+\theta)d\theta, i \neq j$. The normalized cross-correlation is practically limited by the *compression ratio BT* (product between time duration T and bandwidth B) and, in most cases, the desired value is less (i.e., better) than $-30\ dB$.

In the frequency domain, the spectral band occupancy defines the frequency interval in which most of the spectrum of the waveform is allocated, generally taken as the equivalent noise band width, $NBW = \frac{1}{2\pi}\int_0^\infty \left|\frac{H(\omega)}{H_{max}}\right|^2 d\omega$, where $|H_{max}|$ is the maximum amplitude of the frequency response of the filter. Sometimes this item is overlooked, especially when noise-like waveforms are concerned, but it is of paramount importance in most real-world radars.

3. Deterministic waveforms

3.1. Linear frequency modulation (LFM)

Pulse Compression allows the radar designer to play with additional degrees of freedom since the signal duration is decoupled with the *Range resolution*: instead of expression (1), the following relationship holds:

$$\Delta R = c/2B \tag{2}$$

where B is the signal bandwidth. A straightforward, well-known way to generate a signal of duration T, with a carrier f_0, whose spectrum occupies a given band B (large enough to satisfy the resolution requirement, i.e. from $f_0 - \frac{B}{2}$ to $f_0 + \frac{B}{2}$), is the LFM of that carrier in a given time interval T, that is, with an instantaneous frequency:

$$f(t) = \frac{B}{T}t \qquad -\frac{T}{2} \leq t \leq +\frac{T}{2} \tag{3}$$

The resulting time-domain complex envelope signal $s(t)$ has a unit amplitude and, from Eq. (3), a quadratic instantaneous phase:

$$s(t) = \exp\left(j\frac{\pi B}{T}t^2 - j\alpha_0\right) \qquad -\frac{T}{2} \le t \le +\frac{T}{2}, \qquad \alpha_0 = \frac{\pi BT}{2} \tag{4}$$

According to the stationary phase principle [9, 18], for a large enough number of independent samples or product BT (compression ratio), the group delay of an LFM signal is proportional to the instantaneous frequency. The spectrum of $s(t)$ is mostly contained in the interval from $\frac{-B}{2}$ to $\frac{+B}{2}$, and it is *quasi rectangular* (see **Figure 3**) with constant amplitude and linear phase in the bandwidth B (and ideally, zero amplitude outside it).

The resulting output of the matched filter (autocorrelation function) has the shape shown in **Figure 4**. It has a time duration $1/B$ and a (unacceptable) *PSLR* of about 13.2 *dB* below the main

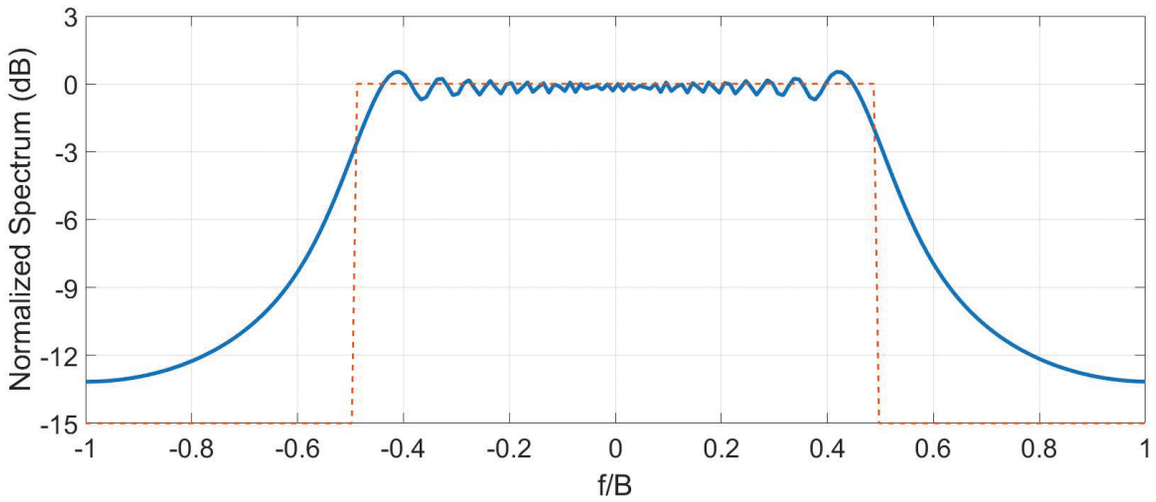

Figure 3. Normalized spectrum of a LFM signal for $BT = 100$. With BT increasing, the spectrum shape is closer and closer to a rectangle (dashed line).

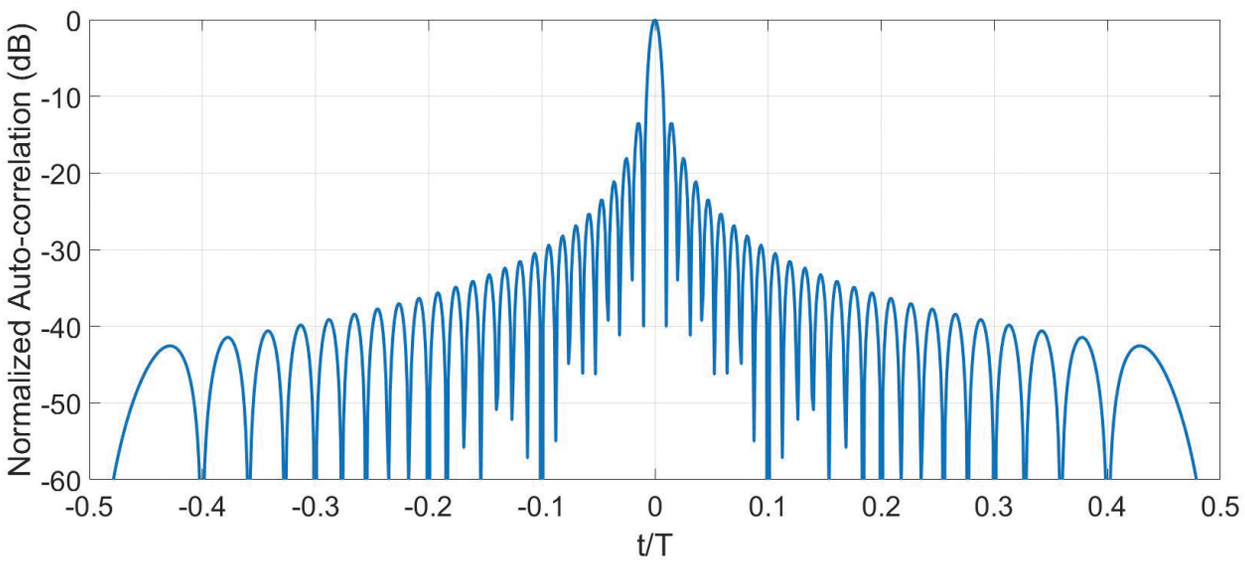

Figure 4. Normalized autocorrelation of a LFM signal with $BT = 100$.

peak. To mitigate the masking effect of nearby targets, the sidelobe level of the autocorrelation function of the transmitted pulse has to reach very low values (<-60 *dB* in some applications such as marine radars) comparable to the two-way antenna sidelobes in *Azimuth*, calling for a more sophisticated frequency modulation law, the non-linear frequency modulation (NLFM) [19].

3.2. Non-linear frequency modulation (NLFM)

In the past, accurate NLFM waveforms were difficult to design, produce, and process. However, the progress of technology now offers the possibility to produce and process high BT, sophisticated NLFM waveforms. The advent of high-speed and high dynamic range Digital-to-Analog-Convertors (DACs) and high-speed large-scale field programmable gate arrays (FPGAs) facilitates generating high-performance precision digital waveforms. Moreover, FPGAs and fast Analog-to-Digital-Convertors (ADCs) allow the direct sampling fairly wide bandwidth signals, and modern high-speed processors allow more sophisticated filtering and detection algorithms to be employed. Historically, the Millett waveform, that is, with a *"cosine squared on a pedestal"* weighting, is the oldest NLFM [19]. By means of the well-known *spectral windows* [9, 18–21], NLFM waveforms can be easily designed. However, this method, relying on the stationary phase principle, is effective in terms of *PSLR* values only when *BT* is large (in practice, greater than a few thousands; see **Figure 5**, where NLFN is obtained by Hamming weighting) and is less effective when a low *BT* is required, as it happens in various civil applications like air traffic control (ATC) radar and marine (or navigation) radar.

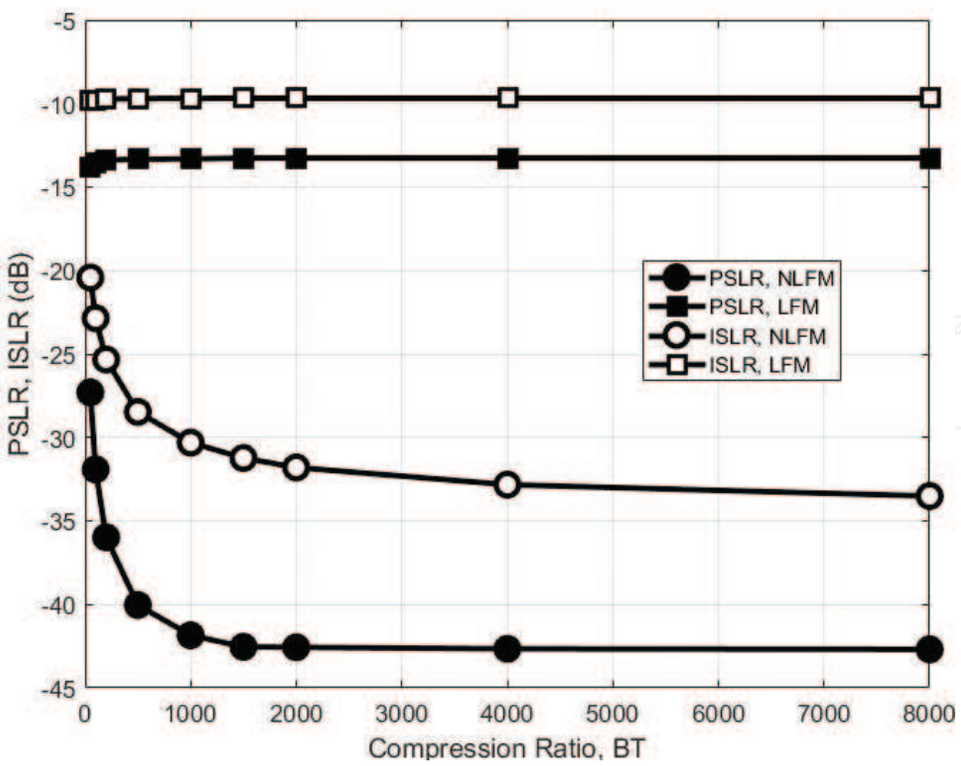

Figure 5. PSLR and ISLR versus the compression ratio (*BT*) for LFM and NLFM (Hamming weighting) signals.

The requirement for further reducing the sidelobe level of the autocorrelation function has been satisfied either by *"tailoring"* the NLFM law or by the use of some sidelobe suppression filter in reception. The latter is used at the expense of losses in the *SNR*, with the additional disadvantage of high complexity and high sensitivity to Doppler frequency that can only be compensated by a bank of filters with another increase of complexity and cost. The former requires a careful design. Let us remember that a waveform with duration T and bandwidth B has $2BT$ degrees of freedom that is completely described by $2BT$ values. Hence, it is clear that for relatively low (tens or hundreds) values of the compression ratio BT, the design is more difficult; see also the NLFM curves of **Figure 5**, with a significant performance degradation for $BT < 500$.

A new design method to cope with the *low compression ratio* problem has been presented in [22, 23], leading to a kind of *Hybrid*-NLFM (HNLFM), whose amplitude, however, is not constant during the duration T of the signal, thus creating implementation problems with the widely used saturated (C-class) power amplifiers. This family of waveforms is enhanced and analyzed in the following.

3.3. Hybrid non-linear frequency modulation (HNLFM)[2]

Let us consider a narrowband signal $x(t) = a(t)\cos[2\pi f_0 t + \phi(t)]$ with power spectrum centered at f_0 and both amplitude modulation (AM) and phase modulation (PM). Its complex envelope is $s(t) = a(t)e^{j\phi(t)}$ where $a(t)$ and $\phi(t)$ denote, respectively, the AM and PM. The Stationary Phase Principle establishes that the amplitude spectrum $|S(\omega_t)|^2$ of the signal $s(t)$ at the instantaneous angular frequency $\omega_t = 2\pi f_t$ can be approximated as:

$$|S(\omega_t)|^2 \cong 2\pi \frac{a^2(t)}{|\phi''(t)|} \tag{5}$$

where $\phi''(t)$ is the second derivative of $\phi(t)$. Hence, the energy spectral density at the frequency $\omega_t = \phi'(t)$ is larger when the rate of change of ω_t is smaller, that is, around the stationary phase point. From Eq. (5), the amplitude modulation function $a(t)$ can be derived for a given spectrum shape (often assumed *Gaussian* or *rectangular* from $-B/2$ to $-B/2$) and for a given instantaneous frequency law $\phi'(t)$:

$$a(t) \cong \sqrt{\frac{1}{2\pi}\left|S\left(\phi'(t)\right)\right|^2 \left|\phi''(t)\right|} \tag{6}$$

However, the applicability of the stationary phase approximation depends on the compression ratio BT. For any compression ratio, a suited frequency modulation function (in radians) can be obtained as a weighted sum of the *non-linear tangent* FM term and the LFM one, hence the name Hybrid-NLFM, [22, 23]:

[2]Part of the results on HNLFM have been funded by Selex-ES (now, Leonardo Company) under the research contract COLB/CTR/2013/20/A.

$$\phi'(t) = \pi B\left\{\alpha \frac{1}{tg\,(\gamma)}\, tg\left(\frac{2\gamma B}{T}\right) + (1-\alpha)\frac{2t}{T}\right\} \tag{7}$$

where $\alpha \in (0,1)$ is the weight, B the sweep frequency interval, γ the non-linear tangent FM rate, and $t \in \left[\frac{-T}{2}, +\frac{T}{2}\right]$ with T denoting the pulse-width. If $s(t)$ is a signal with a Gaussian spectrum $|S(\omega_t)|^2 = \exp\left(\frac{-\omega_t^2}{B^2}\right)$, we may use the optimized values of α and γ, that is, those values that reach the optimum *PSLR*, maximizing the transmission efficiency $\frac{1}{T}\int_{-T/2}^{+T/2} a^2(t)dt$. **Figure 6** shows the resulting normalized amplitude weighting whose loss (with respect to a rectangular pulse) results as low as 0.58 *dB* only. **Figure 7** shows a zoom around $a(t)=1$ of **Figure 6** evidentiating its amplitude ripples of the order of 10^{-3}. In **Figure 8**, the corresponding frequency modulation is shown. **Figure 9** shows the *PSLR* of the matched filter output for this optimized type of waveform (solid line circles). A dramatic improvement with respect to the Millet waveform is clearly seen.

As usual, with BT decreasing, the approximation due to the principle of the stationary phase becomes worse causing an increase in the *PSLR*. However, with $BT = 64$, the *PSLR* (-51 *dB*) is

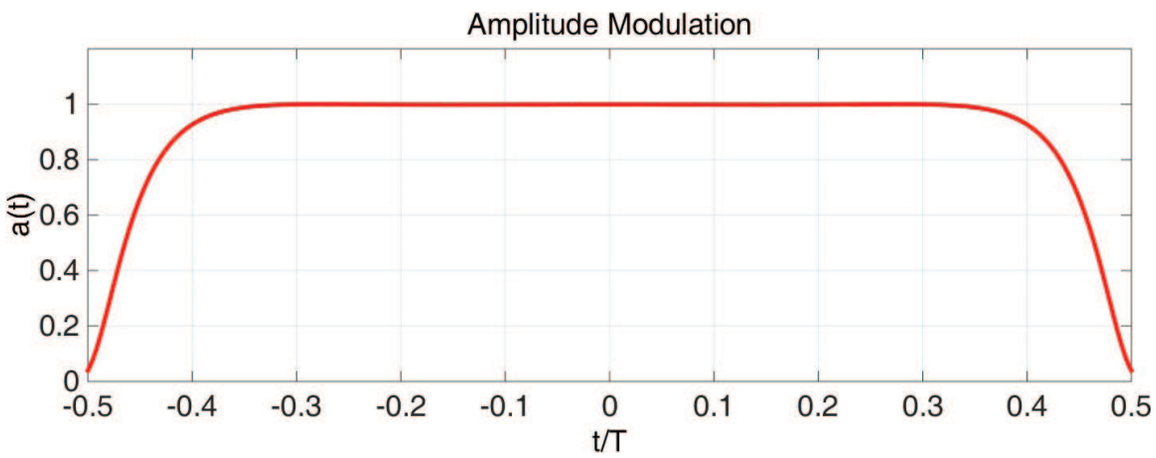

Figure 6. Optimum amplitude modulation for the HNLFM signal.

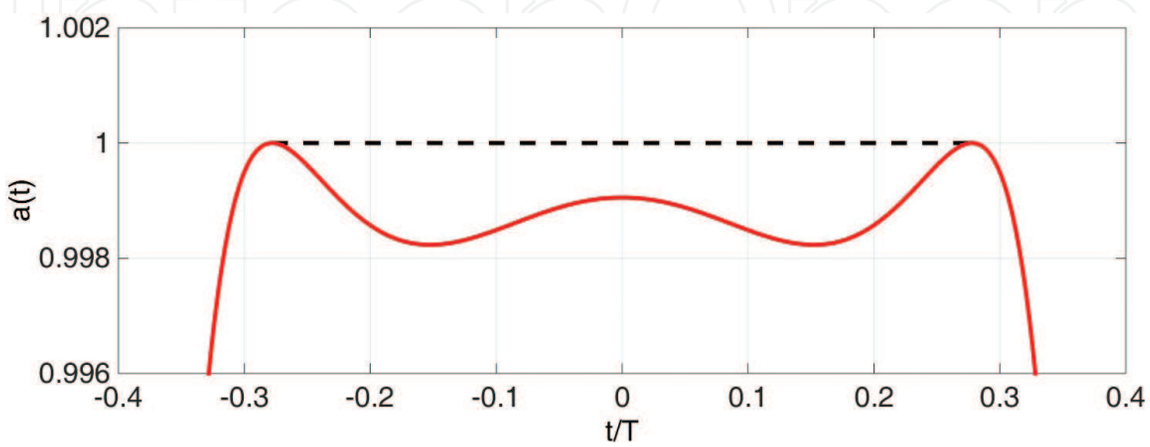

Figure 7. Optimum amplitude modulation for the HNLFM signal, zoom near the unit (solid line).

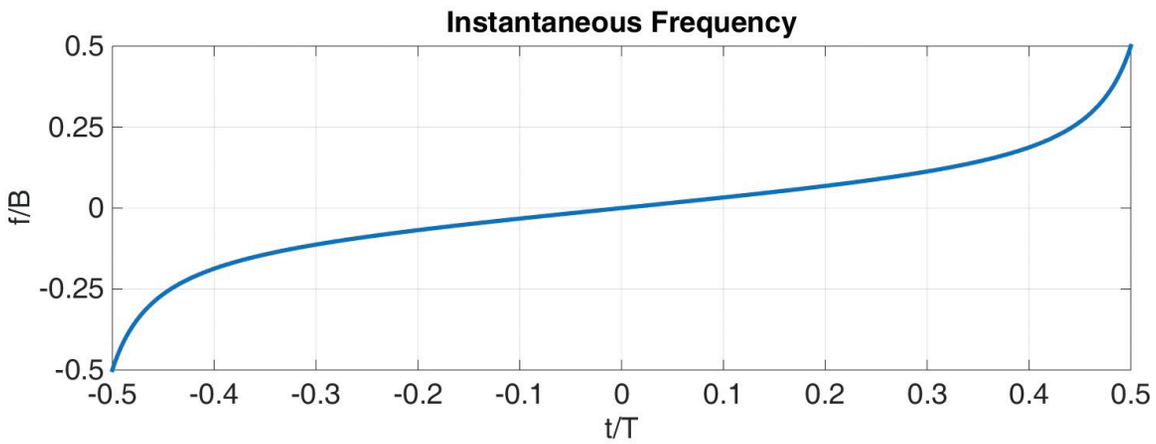

Figure 8. Instantaneous frequency of the HNLFM signal.

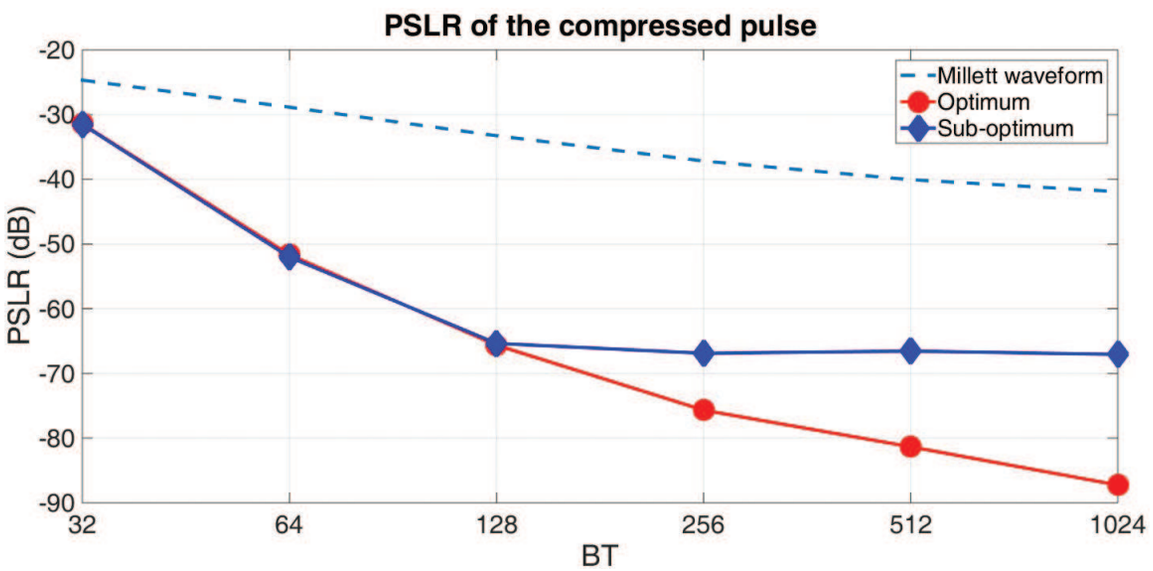

Figure 9. PSLR versus the compression ratio (BT) for HNLFM.

still compatible with many applications and for $BT = 256$ the PSL is -75 dB, suited to most applications. These excellent results (solid line circles in **Figure 9**) are possible *if and only if* the amplitude weighting is strictly the one shown in **Figure 7** (continuous line) and the frequency modulation is the one of **Figure 8**. In practice, it may be hard to practically implement these requirements on $a(t)$, with ripples of the order of 1 over 1000. It is preferable that the amplitude of the transmitted signal should be kept constant (with the power amplifier working in saturation at least in the central part of the pulse). However, this choice leads to increasing the $PSLR$ by 25–30 dB. An improvement can be obtained using a sub-optimum waveform where the ripples shown in **Figure 7** are removed imposing a constant value (unit value), see the dashed line in **Figure 7**. The corresponding $PSLR$ results in only 10–20 dB greater than the optimized signal when $BT \geq 256$ (diamonds in **Figure 9**).

To evaluate the effect due to the radial velocity v_r, supposing $v_r = 250$ *m/s* (900 *km/h*, i.e., 500 *knots*, reasonable limit reached by a civil aircraft) and a compression ratio of 256, in the L or S band, the effect due to Doppler on the output from the matched filter is very limited, particularly on the *PSLR*. Finally, to evaluate the effect of the analog-to-digital conversion, we considered as an input to the waveform generator a digital sequence coded with n bits. In reception, the coefficients of the matched filter are coded with the same number of bits. Varying n (8, 10, 12), as one could expect, a *PSLR* better than −60 *dB* calls for a 10 *bit* quantization, while with 12 bits it is possible to stay very close to the theoretical limit. Using commercial components, the matched filter coefficients are typically quantized at 16 bits, while for the data (I/Q after ADC), 12 bits seem appropriate. So, the quantization should not increase the sidelobes by a significant amount. The good performance of the HNLFM to get very low sidelobes of the compressed pulse, and also for low *BT*, is strictly dependent on the ability of the signal generation and amplification chain, including the RF power amplifier, to faithfully reproduce the amplitude modulation of **Figures 6** and **7**, calling for highly linear A-class amplifiers. Moreover, the available bandwidth is not fully exploited because of the particular frequency law of Eq. (7), which is the main law responsible for the low sidelobe level.

4. Orthogonal waveforms

In MIMO applications [13], M different waveforms (codes) are typically required, where M is the number of the transmit elements. In reception, the orthogonal property of the M transmitted waveforms permits their separation. Neglecting the polarization aspects, orthogonality may be imposed in the *time domain*, in *frequency domain,* or in *signal space*. In most radar applications, obtaining the orthogonality in the signal space is the best choice to avoid potential performance degradation due to the loss of coherence of the target response [24]. Good candidates to design deterministic signals that satisfy the orthogonality requirements are the well-known *"up"* and *"down"* chirp (LFM and NLFM) [14], but in this case, only one pair of signals can be defined. To obtain M pairs (with $M > 1$) of signals, the Costas codes represent a possible solution [25]. Alltop sequences [26] and OFDM signals [27] also can be considered. The main limitation of the OFDM approach is due to the non-constant envelope of the signals, that is, MEPPR <1, meaning that the transmitter does not work at its maximum power.

Another class of waveforms is the *non-deterministic* signals (*random* signal or *noisy waveforms*). Among these, the class of random *phase signals* (with constant amplitude [28], see paragraph 5.1) has two main advantages as compared to the signals introduced before. The former is the possibility to generate a large enough number of orthogonal signals, which is of great importance in MIMO radar systems. The latter is about the detectability; in fact, they are random signals so they place limitations on the detection, the identification, and the eventual spoofing of the signal, an element of great importance in many military applications which require low detectability of the radar system. Finally, the crest factor reaches unity. The random signals, such as the noise waveforms, will be described in Section 5.

4.1. Comparison among orthogonal waveforms

4.2. Up and down LFM and NLFM

For *up* and *down* LFM the amplitude of the cross-correlation has been evaluated in [29]:

$$|r_{12}(t)| = 2\left|\mathcal{F}\left(\sqrt{BT}\left(1-\frac{|t|}{T}\right)\right)\right| \qquad -T < t < +T \tag{8}$$

where $F(\cdot)$ is the *Fresnel Integral* in a complex form: $F(z) = \int_0^z \exp\left(j\frac{\pi}{2}y^2\right)dy$. For the *up* and *down* NLFM, the evaluation of the cross-correlation leads to very complicated expressions and its values are better derived by simulation. **Figure 10** reports the normalized cross-correlation versus the compression ratio BT for LFM and NLFM, the latter obtained supposing a Hamming weighting. The performance limitation due to the compression ratio is clearly shown.

4.3. Costas codes

A Costas code [25], see **Figure 11**, can be obtained dividing the time-frequency plane in M sub-elements (chips) of equal duration t_b and band $\Delta f = 1/t_b$.

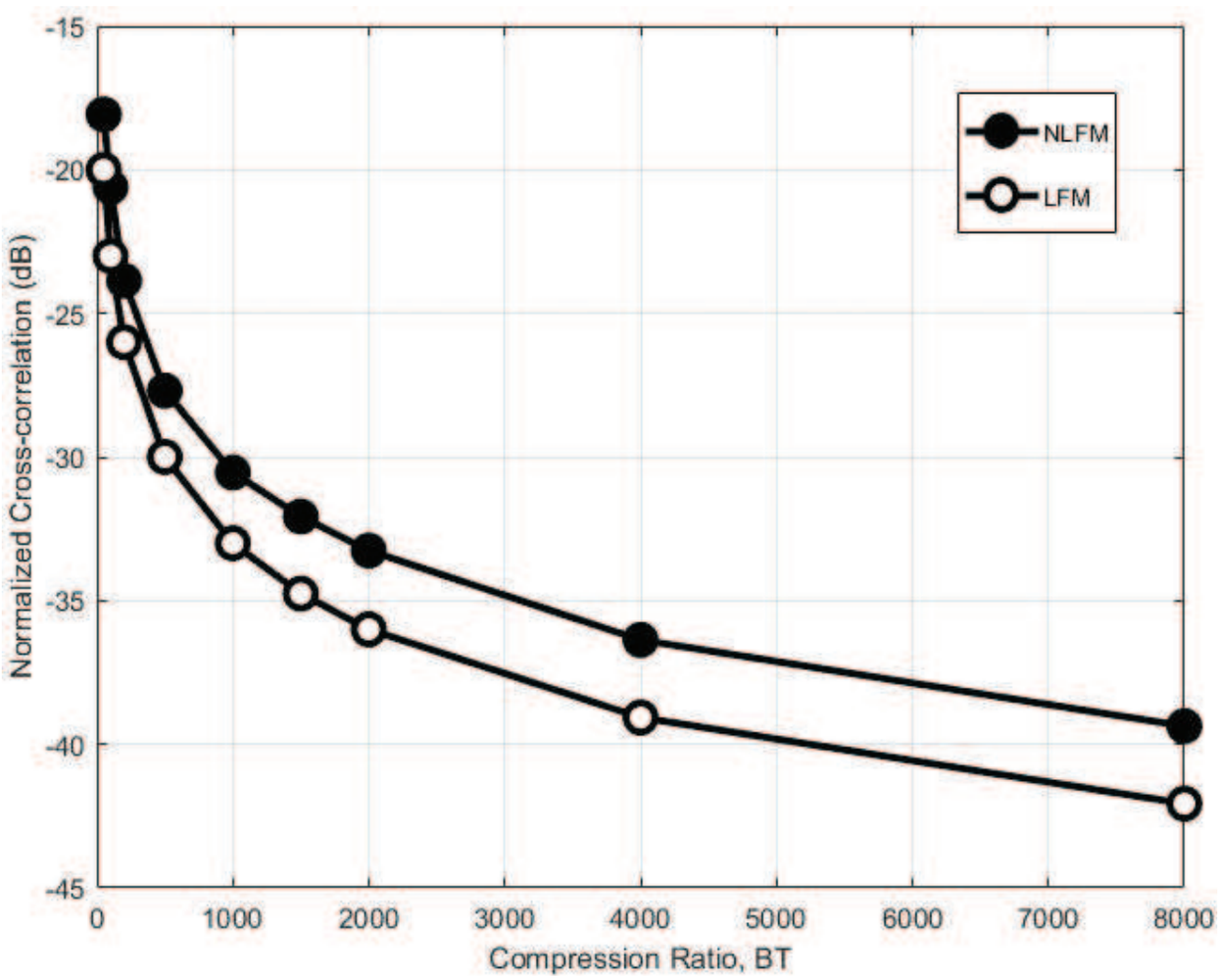

Figure 10. Cross-correlation versus the compression ratio (BT) for LFM and NLFM signals.

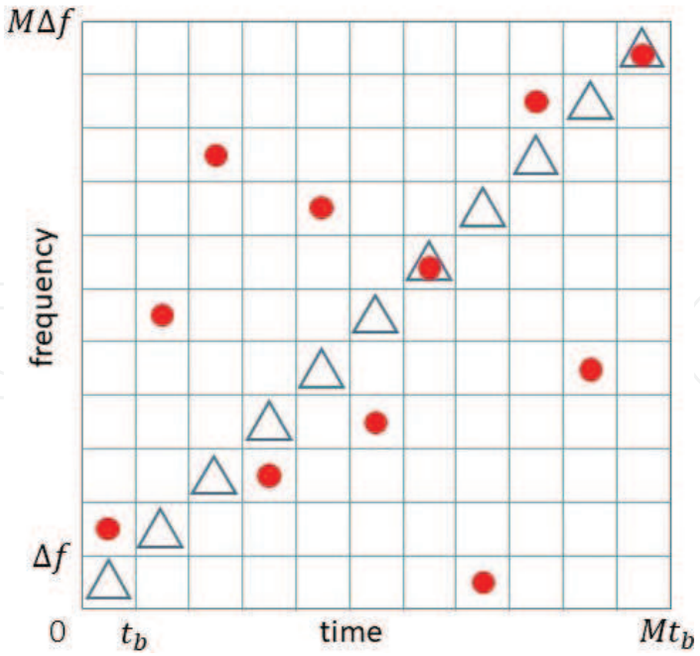

Figure 11. Circles show an example of Costas code with M = 11, hopping sequence: {2, 6, 9, 3, 8, 4, 7, 1, 10, 5, 11}. Triangles show the time-frequency relationship for a discretized Linear FM signal with the same duration and bandwidth.

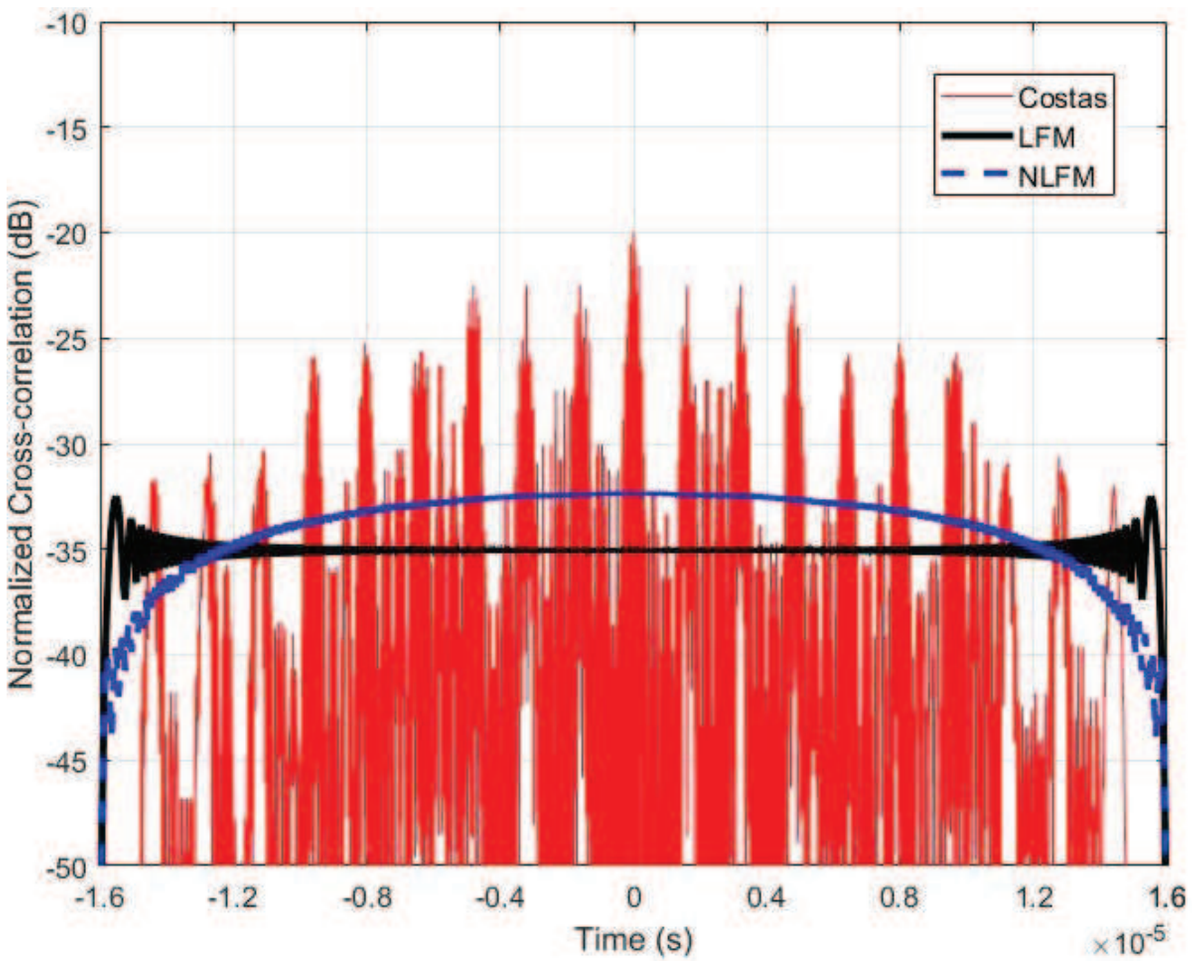

Figure 12. Normalized cross-correlation of a pair of Costas codes (BT = 1600) compared with the ones of LFM and NLFM *up* and *down* signals.

The complex envelope of a Costas signal of length $T = Mt_b$ (M integer) is:

$$s(t) = \frac{1}{\sqrt{Mt_b}} \sum_{m=1}^{M} \exp\left(j2\pi f_m t\right) rect_b\left[t - (m-1)t_b + \frac{T}{2}\right] \tag{9}$$

where t_b is the chip time and $f_m = a_m \Delta f$, where $m = 1, 2, \ldots, M$ is the carrier frequency of the chip m, $a = [a_1, a_2, \ldots, a_M]$ is the sequence of distinct integers between 1 and M defining the particular code (*hopping sequence*) and $rect_b(t)$ is equal to 1 for $0 \le t < t_b$ and 0 elsewhere. The bandwidth is $B = M \cdot \Delta f$ and the resulting compression ratio is M^2. The typical *PSLR* is the same as a linear discrete chirp with the same number of elements M.

A modified Costas signal has been introduced to decrease the sidelobes of the AF at *zero* Doppler as reported in Ref. [30]. **Figure 12** shows the normalized cross-correlation for a pair of Costas codes compared with *up* and *down* LFM and NLFM with the same *BT*, that is, 1600.

5. Random waveforms: Noise radar technology

Noise radar technology (NRT) [15, 31–35] makes use of *pseudo-random* waveforms that are realizations of a Gaussian band-limited random process or transformations of it. These *"pure noise"* realizations, once generated and stored, are not strictly random anymore as they act as deterministic signals with known *PSLR*, *Range* resolution and ambiguity function. The number of different possible realizations to be used is theoretically unlimited (modern pseudo-random numbers generator can reach a period of 2^{1492} [36], as implemented in the MATLAB generator: practically infinity), so that each radar can operate with its own signal, possibly different from the others. For a pure noise waveform, the *PLSR* value does not strongly depend on the amplitude modulation but, rather, on the time-bandwidth product *BT*. The bandwidth being limited by the application context (e.g., about 50 and 200 *MHz* as a maximum, for a marine radar), *BT* may be increased at will by selecting a continuous wave (CW) architecture instead of the pulsed one, keeping unchanged the compression processing (computation of the correlation or of the ambiguity function) at the receiver side. The power can be significantly lowered with respect to an equal-performance pulse radar architecture. Considering a typical maximum *Range* of 150 *km* (80 *NM*) with a *Range* resolution of 150 *m*, a comparison between pulsed HNLFM and CW noise radar can be done while keeping the transmitted energy constant. For this purpose, let us consider the sub-optimal HNLFM (see **Figures 6** and **7**) since the power loss with respect to the optimal amplitude modulation is only 0.58 *dB*. In a CW architecture, the maximum delay due to *Range* is generally set as *one-fourth* of the wave repetition time (WRT), which corresponds to the signal time duration if we neglect the data processing time between consecutive sweeps. Then imposing $\frac{WRT}{4} = \frac{2 \cdot R_{max}}{c}$, for $R_{max} = 150$ *km*, it is required that $WRT = 4000$ μs. Knowing the time duration of the noise signal (WRT_{noise}) and the HNLFM pulse width (T_{HNLFM}), the relationship between the needed peak powers can be evaluated as: $P_{noise} = P_{HNLFM} \cdot \frac{T_{HNLFM}}{WRT_{noise}}$ where P_{noise} and P_{HNLFM} are, respectively, the peak power of CW noise and pulsed radar. With $WRT_{noise} = 4000$ μs and $T_{HNLFM} = 128$ μs, it results as: $P_{noise} = 0.032 \cdot$

P_{HNLFM}. Then, the required power for a CW noise radar is about 15 *dB* lower than the peak power required for a pulsed radar, keeping unchanged the maximum *Range*. Lowering the transmitted power means less solid-state modules and a straightforward RF power production/generation design.

5.1. Unimodular noisy signals

Theoretically a unimodular noisy signal shows a complex envelope with constant amplitude and with a phase $\phi(t)$ being a *zero-mean* Gaussian process with *root mean square (RMS)* σ and density spectrum within the band b. In [28], it has been shown that the normalized autocorrelation function of these signals can be written in a closed-form expression as:

$$R(\tau) = \exp\left\{-\sigma^2\left[1 - \rho(\tau)\right]\right\} \tag{10}$$

where $\rho(\tau)$ is the correlation coefficient of $\phi(t)$. $R(\tau)$ depends on the bandwidth b, on the pulse length T and on the phase fluctuation σ. The bandwidth b is related to the width of the main peak, that is, it determines the *Range* resolution. An increase of T, and consequently of the compression ratio, causes a reduction of the *Range* sidelobe level, whereas the mainlobe width remains fixed, being independent of T. Finally, σ has two different effects. The former is on the sidelobe level: an increase of σ causes a decrease of the sidelobe level and an improvement of the *PSLR*. The latter concerns the resolution. In fact, σ establishes a connection between the bandwidth of the modulated signal and the bandwidth of the modulating signal $\phi(t)$. In more detail, when σ increases, the final bandwidth increases too. As a consequence, a large value of σ gives an improved resolution. In [28], a simple relation between the *RMS* bandwidth of the phase modulated signal (B_{rms}) and the *RMS* bandwidth of the phase modulating noise (b_{rms}) has been found as $B_{rms} = \sigma \cdot b_{rms}$. For the sidelobe suppression, the expression of the autocorrelation function Eq. (10) would show a continuous improvement of the sidelobe suppression as σ increases. Unfortunately, this is not true: the periodic nature of the phase $\phi(t)$ with a folding in the $[-\pi, +\pi]$ interval has been neglected in [28], and in reality, the model can be used only for values of σ much smaller than π.

Considering realistic and correct simulations aimed at a potential application, the best approach generates the signal through a white Gaussian process with its *in-phase* and *quadrature* components (I, Q) that are band limited as desired. The procedure to generate M independent pure noise unimodular band-limited signals is shown in **Figure 13**. The (I, Q) samples, that have to be filtered by the frequency window $H(f)$, are $\{x_i\}_{i=1}^{N}$ where N is the number of generated samples and x_i is the ith complex (I, Q) sample.

After the frequency domain windowing, the signal amplitude is saturated to the maximum value through a Zero-Memory-Non-Linear (ZMNL) transformation, while the phase is kept unchanged. Since the (I, Q) samples come from a random process, at each run the algorithm provides different realizations having the same average performances in terms of *PSLR* and cross-correlation level, while the *Range* resolution only depends on the used $H(f)$. Unimodular band-limited (with a rectangular window) pure noise shows a *Range* resolution similar to the

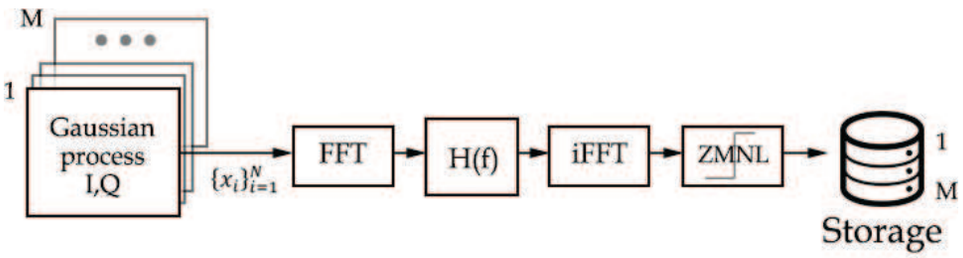

Figure 13. Scheme to generate M independent pure noise unimodular band-limited signals.

LFM with the same band, and the secondary lobes are slightly fluctuating (the *PSLR* is comparable to the LFM). For the far lobes, the *PSLR* is empirically related to the *BT* by:

$$PSLR_{dB} = -10 \cdot log_{10}(BT) + k \tag{11}$$

with k of the order of 10–13 dB, which corresponds to -23 dB for $BT = 4000$.

The cross-correlation level between two independently generated pure noise signals is of the same level as the autocorrelation sidelobes, excluding the central zone. This fact calls for sidelobe-suppression methods. Sidelobe suppression of both the autocorrelation and cross-correlation function of a set of M waveforms (with $M > 1$ and of the order of a few units or a few tens) is a relevant problem in a MIMO radar, whose receivers have to discriminate, after each matched filter, the *mth* signal among the others. So, M *"orthogonal"* waveforms are required [13] for MIMO radar and for space-time coding or *"colored"* transmission [16].

5.2. Range sidelobe suppression algorithms

Many approaches have been used in the past years to cope with the *Range* sidelobe problem, starting from the time (or frequency) weighting of the received signal. Algorithms are available to generate signals with suitable autocorrelation characteristics without the need for sidelobe suppression in reception. However, using the generation algorithms, significant complexity is demanded to the generation side in terms of computational burden to achieve a "useful" waveform. In any case, this issue can be trivially overcome by offline methods, generating a large enough set of noisy waveforms ready to be transmitted and stored in mass memory.

A first method to reduce the sidelobes of the unimodular noisy signals uses an iterative procedure based on alternative projections in the frequency and in time domain [15]. Using this approach, if the compression ratio is greater than 5000 the mean *PSLR* reaches -30 dB, however it remains limited to -36 dB for $BT = 30{,}000$. Regarding the cross-correlation of a pair of noise signals, it is comparable with the ones of the LFM and NLFM.

A second approach, starting from a random process realization (**Figure 13**), runs in order to minimize a certain objective function with defined constraints. In this case, the objective function is the *PSLR* and the constraints are the limited bandwidth and the unity amplitude needed to fully exploit the amplifier. Often, due to convergence considerations, the *ISLR* is

minimized instead of the *PSLR* because the former is an integrated value over all the sidelobes region while the latter is only a local value that can rapidly change point by point.

A powerful sidelobe suppression algorithm family, Cyclic Algorithm New (CAN), described in [17] provides several interesting ways to approach the suppression problem. To suit to particular needs, the *Radarlab* group in Tor Vergata University developed a new algorithm to generate noisy waveforms having a limited bandwidth and a unimodular amplitude, with the possibility to tune the suppressed zone length depending on the particular application [37].

The main idea is to minimize the difference between the obtained and the desired autocorrelation functions through a process that runs cyclically until a stop criterion is satisfied, for example, the difference between two consecutive steps is less than a given threshold. The constraints to be satisfied within this minimization lead to different algorithms belonging to the wide CAN family. These constraints can be the unit amplitude, the number of suppressed sidelobes, as well as the mainlobe width (i.e., the required bandwidth) or others.

For this purpose, the CAN family also provides a MIMO version for the algorithms in which the quantity to be minimized is the difference between the obtained and the desired covariance matrix. The main drawback of the CAN algorithms is their inability to manage the bandwidth increase, as the mainlobe of the signal generated by using the CAN algorithm is very narrow. In fact, these algorithms converge to a deep sidelobe suppression at the expense of a full-Nyquist occupied bandwidth, which unfortunately is not suitable for applications in which spectrum regulations must be met. Only one CAN algorithm (named SCAN, Stopband-CAN) is able to manage the spectrum constraint. If the SCAN is applied to generate noise unimodular signals with $BT = 4096$ and $B = 1\ MHz$, the related aperiodic autocorrelation is shown in **Figure 14**.

Keeping BT unchanged, the SCAN algorithm improves the *PSLR* by about 20 dB with respect to the unimodular noise from which the algorithm starts. The mainlobe is kept wide since the SCAN spectrum is well shaped within the required 1 MHz bandwidth. The drawback of the SCAN algorithm is that the sidelobes close to the mainlobe are still quite high. To overcome

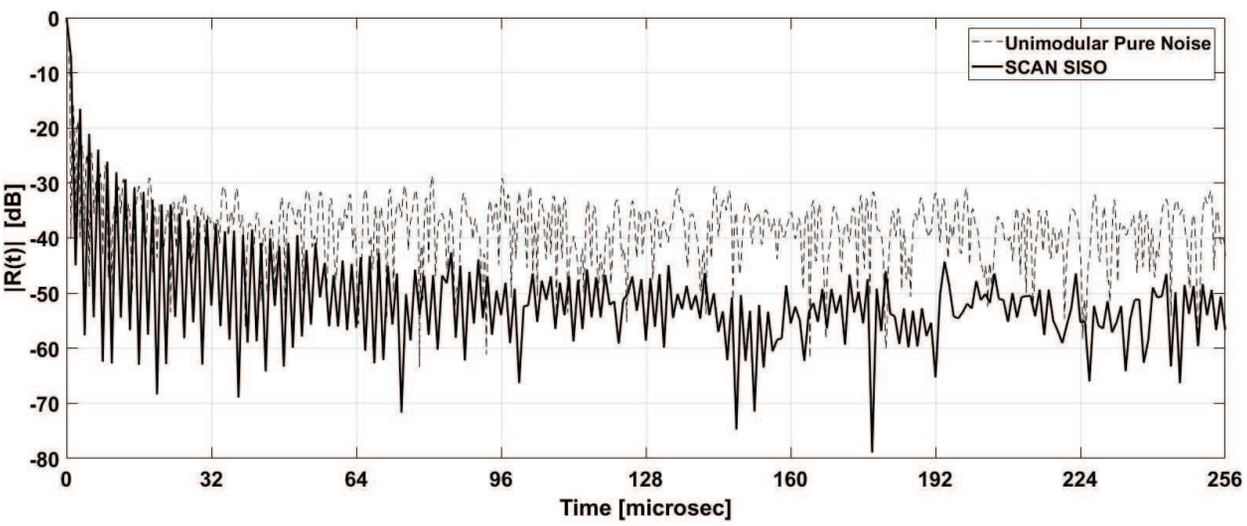

Figure 14. Unimodular noise compressed pulse: SCAN. $B = 1\ MHz$ and $T = 4096\ \mu s$.

the issue, our group has developed the Band Limited Algorithm for Sidelobes Attenuation (BLASA) algorithm [37] whose typical result is shown in **Figure 15**. It comes from the CAN idea and provides very low sidelobes even in the area close to the mainlobe. It is called Single Input, Single Output (SISO) because a single waveform is generated at each run. The BLASA SISO spectrum is still well shaped within the allowed 1 *MHz* bandwidth, providing a *Range* resolution of 150 *m*.

Being a SISO algorithm, BLASA does not lower the cross-correlation level between two independently generated waveforms. Hence, their cross-correlation is at the same level as the initial unimodular pure noise.

As in the CAN family, even for the BLASA SISO, a MIMO version exists [37] which is able to jointly generate a number M of waveforms at each run, that is, M signals belonging to the same set. The BLASA MIMO is developed to manage the suppression of both auto and cross-correlation functions, still keeping the bandwidth limited. Due to the limited number of samples that BLASA MIMO can manipulate, the joint suppression region in cross and auto-correlations cannot be as long as the whole length of the pulse. The length of the suppressed zone depends on the number M of waveforms in the generated set: the lower M, the longer the suppressed length. Moreover, the suppressed zone length depends on the amplitude constraint: it increases if amplitude modulation is allowed while it decreases if the unimodular constraint is applied. Hereafter, only the unimodular case will be considered. The limited length of the suppressed zone represents a valid tool to mitigate the clutter effect, especially near the mainlobe, that is, the target's closest *Range* cells. Because of the narrow -3 *dB* bandwidth, the mainlobe is four times wider than the expected 150 *m*, which corresponds to a 1 *MHz* bandwidth. Nevertheless, this behavior is deterministic and can be overcome by choosing properly the signals' occupied bandwidth. The big advantage of the BLASA MIMO pseudorandom signals with respect to the deterministic HNLFM is the possibility to average coherently the *Range* sidelobes in the *Azimuth*. In fact, if the transmitted waveform changes each Waveform Repetition Time within the dwell time, the averaged compressed pulse presents a sidelobe level reduced by the quantity: $\Delta SL = 10 \cdot log_{10}(L)$ where ΔSL is the lowering in

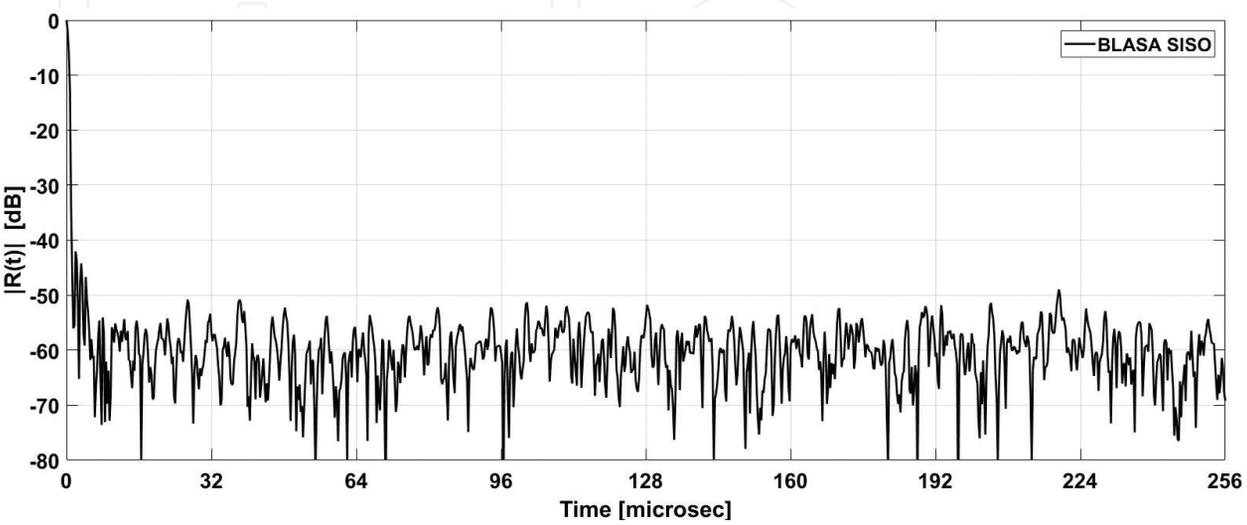

Figure 15. Unimodular noise compressed pulse: BLASA. $B = 1$ *MHz* and $T = 4096$ μs.

Algorithm	MIMO version	Sidelobe level and suppression interval	$\frac{B_{TOT}}{B_{-3dB}}$	Amplitude modulation
HNLFM	No	$-67\ dB$ at $BT = 4096$	400%	Pseudo trapezoidal AM
Unimodular Noise	No	$-23\ dB$ at $BT = 4096$	100%	Unimodular
SCAN	No	$-45\ dB$ at $BT = 4096$ (within 15%)	100%	Unimodular
BLASA SISO	No	$-50\ dB$ at $BT = 4096$	100%	Unimodular
BLASA MIMO	Yes	$-30\ dB$ at $BT = 256$ (within 12%), unimodular amplitude with $M = 2$	400%	Unimodular

Table 1. Comparison of algorithms.

the sidelobe level with respect to the not-averaged case and L is the number of coherently integrated returns.

Summing up all the considered waveforms, **Table 1** shows their comparison. Each algorithm is checked to verify whether it allows a MIMO version, the level of the sidelobes, the frequency occupancy, and its capability to be coherently integrated.

The column "MIMO version" refers to the capability of jointly generated M waveforms with a cross-correlation level comparable to the auto-correlation level. The frequency occupancy $\frac{B_{TOT}}{B_{-3dB}}$ gives the information of how much the mainlobe is enlarged by the algorithm.

6. Conclusions

Waveform design is a critical component in the design of an effective and efficient radar system. Various types of radar signals have been proposed and analyzed for over half a century, resulting in extensive literature on the subject matter. This chapter, after an overview of the various proposed waveforms, examined in more detail two particular classes of radar signals, that is a deterministic and a random one. The former is based on non-linear frequency modulation of the radar pulse, which, with a suited amplitude modulation added, can reach extremely low-*Range* sidelobes in the absence of Doppler shift. The latter class is used in the novel *noise radar technology*, still at research stage, where a suited tailoring of the noisy waveforms grants a fairly low sidelobe level. Pro and cons of both approaches are also discussed.

Author details

Gaspare Galati[1,2]* and Gabriele Pavan[1,2]

*Address all correspondence to: gaspare.galati@uniroma2.it

1 Tor Vergata University, Department of Electronic Engineering, Rome, Italy

2 CNIT, Interuniversity Consortium for Telecommunications, Italy

References

[1] Skolnik M.I. Introduction to Radar Systems. 3rd ed. New York: McGraw-Hill Education; 2015

[2] Nathanson F.E., Reilly J.P., Cohen M.N. Radar Design Principles: Signal Processing and the Environment. Mendham, New Jersey: Scitech Pub; 1999

[3] Turin G.L. An introduction to matched filters. IRE Transactions on Information Theory. 1960;**6**(3):311-329. DOI: 10.1109/TIT.1960.1057571

[4] North D.O. An analysis of the factors which determine signal/noise discrimination in pulsed carrier systems. Proceedings of the IEEE. 1963;**51**(7):1016-1027. DOI: 10.1109/PROC.1963.2383

[5] Galati G. 100 Years of Radar. 1st ed. Springer International Publishing; 2016. DOI: 10.1007/978-3-319-00584-3

[6] Galati G., van Genderen P. Special section on some less-well-known contributions to the development of radar: From its early conception until just after the second world war. The Radio Science Bulletin. 2016;**358**:12–108

[7] Barker R.H. Group synchronizing of binary digital systems. Communication Theory. London: Butterworth Sci. Pub; 1953:273-287

[8] Klauder J.R., Price A.C., Darlington S., Albefsheim W.J. The theory and design of chirp radars. Bell System Technical Journal. 1960;**39**:745-808

[9] Cook C.E., Bernfeld M. Radar Signals—An Introduction to Theory and Application. Norwood, MA, USA: Artech House; 1993

[10] Pioneer Award IEEE Trans. Aerospace and Electronic Systems. 2010;**46**:2139-2141

[11] Yanovsky F. Radar development in Ukraine. In: International Radar Symposium (IRS 2014); 16–18 June 2014; Gdansk, Poland; 2014. DOI: 10.1109/IRS.2014.6869179

[12] Woodward P.M. Probability and Information Theory with Applications to Radar. London: Pergamon Press; 1953

[13] Li J., Stoica P. MIMO Radar Signal Processing. Wiley/IEEE Press; 2008

[14] Galati G., Pavan G. Orthogonal and complementary radar signals for multichannel applications. In: EuRad 2011; 12–14 October 2011; Manchester (UK). 2011. pp. 178–181

[15] Galati G., Pavan G. On the Design of Waveforms for noise-MIMO radar. In: Noise Radar Technology, NRT-2012; 27-29 September 2012; Yalta, Crimea (Ukraine). 2012. p. 1–7

[16] Barbur G., Aubry P., Le Chevalier F. Space-time radar waveforms: Circulating codes. Hindawi Journal of Electrical and Computer Engineering. 2013. DOI: 10.1155/2013/809691

[17] He H., Li J., Stoica P. Waveform Design for Active Sensing Systems—A Computational Approach. Cambridge University Press; 2012

[18] Levanon N., Mozeson E. Radar Signals. Hoboken, NJ, USA: John Wiley & Sons; 2004

[19] Millett R.E. A matched-filter pulse-compression system using a nonlinear FM waveform. IEEE Transactions on Aerospace and Electronic Systems. 1970;**AES-6**:73-77

[20] Davenport W.B., Root W.L. An Introduction to the Theory of Random Signals and Noise. Wiley-Interscience; 1987

[21] Nuttall H.A. Some windows with very good sidelobe behavior. IEEE Transactions on Acoustics, Speech, and Signal Processing. 1981;**ASSP-29**(1):84-91

[22] Collins T., Atkins P. Nonlinear frequency modulation chirps for active sonar. IEE Proceedings Radar, Sonar and Navigation. 1999;**146**:312-316

[23] Zhiqiang G., Peikang H., Weining L. Matched NLFM pulse compression method with ultra-low sidelobes. In: 5th European Radar Conference; 30–31 October 2008; Amsterdam, The Netherlands. 2008. pp. 92–95

[24] Galati G., Pavan G. Range sidelobes suppression in pulse-compression radar using Golay pairs: Some basic limitations for complex targets. IEEE Transactions on Aerospace and Electronic Systems. 2012;**48**(3):2756-2760

[25] Costas J.P. A study of a class of detection waveforms having nearly ideal range-Doppler ambiguity properties. Proceedings of the IEEE. 1984;**72**(8):996-1009

[26] Alltop W.O. Complex sequences with low periodic correlations. IEEE Transactions on Information Theory. 1980;**IT-26**(3):350-354

[27] Krasnov O.A., Wang Z., Tigrek R.F., van Genderen P. OFDM waveforms for a fully polarimetric weather radar. In: ESAV'11; 12-14 September 2011; Capri (Italy). 2011. pp. 69–75

[28] Axelsson R.J. Noise radar using random phase and frequency modulation. IEEE Transactions on Geoscience and Remote Sensing. 2004;**42**(11):2370-2384

[29] Galati G., Pavan G. Waveform radar design using orthogonal and complementary codes. Prace Przemysłowego Instytutu Telekomunikacji. 2010;**145**:28-44

[30] Levanon N., Mozeson E. Modified Costas signal. IEEE Transactions on Aerospace and Electronic System. 2004;**40**(3):946-953

[31] Stove A., Galati G., Pavan G., De Palo F., Lukin K., Kulpa K., Kulpa J.S., Maślikowski Ł. The NATO SET-184 noise radar trials 2016. In: 17th International Radar Symposium; 10–12 May 2016; Krakow (Poland). 2016. DOI: 10.1109/IRS.2016.7497327

[32] Galati G. Coherent Radar. Patent PCT/IC2014/061454 ed. 15 May 2014

[33] Galati G., Pavan G., De Palo F., Stove A. Potential applications of noise radar technology and related waveform diversity. In: 17th International Radar Symposium. 10–12 May 2016; Krakow (Poland). 2016. DOI: 10.1109/IRS.2016.7497329

[34] Stove A., Galati G., De Palo F., Wasserzier C., Erdogan Y.A., Kubilay S., Lukin K. Design of a Noise Radar Demonstrator. In: 17th International Radar Symposium; 10–12 May 2016; Krakow (Poland). 2016. DOI: 10.1109/IRS.2016.7497328

[35] Kulpa K. Signal Processing in Noise Waveform Radar. Norwood, MA, USA: Artech House; 2013. ISBN 9781608076611.

[36] Marsaglia G., Tsang W.W. The ziggurat method for generating random variables. Journal of Statistical Software. 2000. DOI: 10.18637/jss.v005.i08

[37] De Palo F. Noise Radar Technology–Waveforms, Architectures, Application Cases [Dissertation]. Rome: Tor Vergata University; 2017. ISBN 978-88-90348259

IntechOpen